ACCEPTED VERSION

M.J.Evans, J.A.M.Sidey, J.Ye, P.R.Medwell, B.B.Dally, E.Mastorakos
Temperature and reaction zone imaging in turbulent swirling dual-fuel flames
Proceedings of the Combustion Institute, 2019; 37(2):2159-2166

© 2018 The Combustion Institute. Published by Elsevier Inc. All rights reserved.

This manuscript version is made available under the CC-BY-NC-ND 4.0 license
http://creativecommons.org/licenses/by-nc-nd/4.0/

Final publication at: http://dx.doi.org/10.1016/j.proci.2018.07.076

PERMISSIONS

https://www.elsevier.com/about/our-business/policies/sharing

Accepted Manuscript

Authors can share their accepted manuscript:

[24 months embargo]

After the embargo period

- via non-commercial hosting platforms such as their institutional repository
- via commercial sites with which Elsevier has an agreement

In all cases accepted manuscripts should:

- link to the formal publication via its DOI
- bear a CC-BY-NC-ND license – this is easy to do
- if aggregated with other manuscripts, for example in a repository or other site, be shared in alignment with our hosting policy
- not be added to or enhanced in any way to appear more like, or to substitute for, the published journal article

17 May 2021

http://hdl.handle.net/2440/118302

Temperature and Reaction Zone Imaging in Turbulent Swirling Dual-Fuel Flames

M.J. Evans[a,*], J.A.M. Sidey[b], J. Ye[a,c], P.R. Medwell[a], B.B. Dally[a], E. Mastorakos[b]

[a]*School of Mechanical Engineering, The University of Adelaide, South Australia, 5005, Australia*
[b]*Hopkinson Laboratory, Engineering Department, University of Cambridge, CB2 1PZ, United Kingdom*
[c]*School of Aerospace, Mechanical and Mechatronic Engineering, The University of Sydney, New South Wales, 2006, Australia*

Abstract

Gaseous and liquid dual-fuel flames present both a practical approach to emissions reduction and a challenge to current state-of-the-art combustion modelling. This paper uses simultaneously imaged temperature and normalised OH signal fields to investigate flame structure and provide experimental data for model validation across a range of swirl-stabilised n-heptane spray flames. These data are obtained by non-linear excitation regime two-line atomic fluorescence (NTLAF) of indium, and planar laser-induced fluorescence (OH-PLIF), respectively. Swirling gas streams are varied by flowrate (63–88% of blow-off), premixed equivalence ratio (including air-only), and by type of gaseous fuel (natural gas and hydrogen). Results are used to describe how hot combustion products interact with the fuel spray: heating and diluting the region above the apex of the spray cone at low air flowrates, but

*Corresponding author. E-mail: m.evans@adelaide.edu.au, Tel.: +61 8 8313 5460, Fax: +61 8 8313 4367.

July 26, 2018

drawing fuel into outer branches of the flame with increasing air flowrates. Adding natural gas to the swirling air stream, at a concentration below the lean flammability limit, gives rise to a temperature increase in the outer branches with little effect on the hot region above the apex of the spray, along the burner centreline. The size of this region is significantly reduced, however, using hydrogen. As the concentration of gaseous fuel increases towards the lean flammability limit, peak temperatures shift towards the outer branch of the flame. Exceeding the lean flammability limit, an additional reaction zone begins to form in the premixed swirling stream, adjacent to the outer branch of the swirl flame. Stable outer branches of the swirl flame, however, become less prevalent and the peak temperatures of the spray flame return to burner centreline. This study provides insight into the complex behaviour of dual-fuel flames, a complementary dataset to related, PLIF-only, studies and validation data for the development of numerical modelling tools.
Keywords: Spray, Swirl, Dual-fuel, Heptane, Hydrogen

---

1. Introduction

Combustion of liquid fuels is the cornerstone of modern aero-engine propulsion systems. The demand for non-conventional, bio-derived fuels [1] and improved combustor designs, such as staged configurations [2–4], has driven research towards a better understanding of the fundamental aspects of spray combustion. In the effort to improve the wider understanding of turbulent spray combustion, flames in a swirling spray burner [2, 5–7] have been selected as target cases for the Workshop on Turbulent Combustion of Sprays (TCS).

Experimental studies of extinction and heat release rate in swirl stabilised, n-heptane (n-C_7H_{16}) spray flames have previously focussed on investigating flame structure and behaviour approaching blow-off conditions [5, 6]. These studies demonstrated a lower propensity for 'holes' in the flame sheet, compared with CH_4 flames [5], and large variations in the structure of local, rich heat-release zones as a result of high local turbulence intensities [6]. Whilst the qualitative trends and lift-off heights from these studies are available for assessing the predictive quality of spray combustion models, they could not provide quantitative validation data.

Multi-fuel combustion has been proposed for both emissions reductions in conventional diesel engines [8, 9], or the flexibility to switch between gaseous and liquid fuels during continuous operation [10]. Flame structure of dual-fuel ethanol sprays, with a swirling premixed methane/air stream in a confined burner, have been shown to be dependent on the flammability of the premixed gaseous stream [2]. In this configuration, flames with very lean gaseous streams exhibited a central flame over the bluff body, confined by

the swirling stream [2]. This extended further downstream into the burner recirculation zone with increasing CH_4, which simultaneously decreased the available of O_2 [2]. Cases with premixed (pmx) streams richer than the lean flammability limit (LFL) of CH_4 ($\Phi_{pmx} > \Phi_{LFL} = 0.5$) exhibited two distinct, lean flame regions on either swirler, suggesting two separate, interacting flames [2].

Numerical studies of multi-inlet combustion systems with complex fuels require finite-rate modelling approaches with the capacity to transport molecular species, such as PDF methods [11] or the Eddy Dissipation Concept (EDC) [12], or streams which are appropriate for mixture-fraction-based approaches. As such, previous experimental studies of ethanol sprays emanating into air/methane mixtures [2] pose a significant challenge for mixture-fraction-based models. To simplify the evaluation of multiple, interacting mixture fractions, n-heptane and H_2 were selected as the primary fuels for the current study. This ensured that all atomic O and N originated from the swirling stream, and all atomic C originated from the main fuel spray. This combination was complemented by mixtures of air/natural gas in the swirling stream to compare against previously identified trends in the ethanol and air/methane system [2].

The structures of swirling spray-only and dual fuel n-heptane flames are investigated in this study. Natural gas and H_2 are added alternatively into the swirling stream to independently study the effects on flame temperature and structure. This is done through simultaneous planar laser-induced fluorescence of the hydroxyl radical (OH-PLIF) and non-linear excitation regime two-line atomic fluorescence (NTLAF). Spatially correlated images

are analysed to study the shift in peak temperature regions and reaction zone structures with varying swirler air flowrates and in dual-fuel flames. This work will additionally provide experimental data for validating simulations of flames with the vaporisation of a complex liquid fuel, with both diffusion and partially premixed regions and significant local dilution.

2. Experimental Setup

2.1. Experimental Conditions

The burner used in this study has previously been used to study dual-fuel ethanol/CH_4 flames [2] and the blow-off of *n*-heptane flames experimentally [6] and numerically [13]. Liquid *n*-heptane issued from an atomising nozzle at 0.27 g/s to produce a hollow cone spray with a 60°cone angle. The nozzle was centred in a 25-mm diameter conical bluff body, in a concentric, annular swirler with an outer diameter of 37-mm and with a swirl number of 1.23 [2]. The flow was confined by quartz plates with inner dimensions of 97 × 97 mm square section, extending 150 mm downstream. Laminar, vertical film cooling of ∼2 m/s was applied to the exterior faces of the quartz burner walls to mitigate damage during data collection.

The constant flowrate of 0.27 g/s of *n*-heptane was measured through a variable area, triflat rotameter with an estimated nominal accuracy of 4%. This included 5% ethanol, which was required to dissolve the $InCl_3$ for the non-linear excitation regime two-line atomic fluorescence (NTLAF) measurements. Gaseous flowrates through the annular swirler were controlled with digital mass flow controllers with nominal accuracies of within 2% of the set value. The flowrates for the measured cases are given Table 1, along with the Φ_{pmx} and heat input from the premixed stream (Q_{pmx}), where 'N'

Table 1: Experimental conditions, flowrate of n-heptane was held at 0.27 g/s. 'N' denotes premixed natural gas, 'H' denotes premixed H_2.

Case	Φ_{pmx}	$\frac{\Phi_{pmx}}{\Phi_{LFL}}$	Q_{pmx} (kW)	U_{pmx} (m/s)
S1	0	-	0	14.3
S1N1[a]	0.18	0.28	6.1	14.6
S1H1[a]	0.03	0.25	1.1	14.4
S1H2	0.08	0.75	3.2	14.7
S1H3	0.16	1.57	6.6	15.2
S3[b]	0	-	0	18.5
S3N1[c]	0.14	0.28	6.1	18.8
S3H1	0.02	0.19	1.1	18.7
S3H2	0.06	0.58	3.2	19.0
S3H3	0.12	1.20	6.6	19.4
S4[d,e]	0	-	0	20.0

[a] $\Phi_{LFL} = 0.1$ for H_2 [14] and 0.5 for CH_4 [2], where Φ_{LFL} is the lower flammability limit of the swirler stream mixture

[b] Corresponds to 'S1' in study with ethanol [2]

[c] Corresponds to 'S1P1' in study with ethanol [2]

[d] Approximately corresponds to 'H1S2' in [6]

[e] 98% air, 2% N_2, by volume (current study)

denotes the addition of natural gas (NG: 92.0% CH_4, 4.2% C_2H_2, 0.2% larger hydrocarbons, 2.6% CO_2, <1% N_2, by volume) to the swirler, and 'H' denotes premixing with H_2. All 'S1' cases and 'S3' cases have the same air flowrate, whilst 'H3' and 'N1' cases were chosen to have similar Φ_{pmx} and Q_{pmx}.

2.2. Experimental Techniques

Planar thermography was performed using non-linear excitation regime two-line atomic fluorescence (NTLAF) of indium [15, 16]. The optical set-up for the planar NTLAF thermography imaging was similar to previous studies [17]. Thermography through NTLAF is performed on indium seeded into the

liquid fuel stream as $InCl_3$ at a concentration of 100 ppm. Laser sheets with wavelengths tuned to the indium transitions at 410.18 nm and 451.13 nm were produced by two dye lasers (Quantel TDL90), and used to pump the ground and thermally excited states (with electronic energy difference ΔE_{10}) of atomic indium. The wavelength near 410 nm was produced by mixing the 1064 nm output of a narrow linewidth, amplified Nd:YAG laser (Quantel YG981) and the 667 nm dye laser output, pumped by the frequency doubled output of the same Nd:YAG laser. The frequency doubling stage of the pump laser was tuned to maximise the energy of the 410 nm output. The wavelength near 451 nm was produced by direct pumping in the second dye laser using the frequency tripled output of a dedicated Nd:YAG laser (Quantel Brilliant B). A total of 250 image pairs of Stokes and Anti-Stokes signals were recorded using two ICCD cameras (Princeton PI-Max 4) imaged through a single $f_{\#}1.2$ lens and a custom-made dichroic beam splitter arrangement. Raw images were filtered with a two-dimensional 5×5 median filter prior to image matching and quantification. The in-plane spatial resolution of the matched, filtered images was estimated to be 70 μm/pixel. This was determined through the imaging of a target at the same plane as the laser sheets. This is better than the sheet thickness of 400 μm, which is the limiting factor in determining the optical resolution. The relative strengths of the Stokes and Anti-Stokes signals, F_{21} and F_{20} respectively, are used to determine the gas-phase temperature, T, through Eq. 1:

$$T = \frac{\Delta E_{10}/k}{\ln\left(F_{21}\left(1+\frac{C_S}{I_{20}}\right)\right) - \ln\left(F_{20}\left(1+\frac{C_A}{I_{21}}\right)\right) + C_T} \tag{1}$$

In Eq. 1, I_{20} and I_{21} are the energy of the incident Stokes and Anti-Stokes laser beams, k is the Boltzmann constant. The calibration constants, C_A, C_S and C_T were determined daily using a premixed laminar flame similar to that described previously [15–17]. This technique is valid for $\Phi > 0.8$ and at temperature above 800 K [15], with a single-shot accuracy within 100 K and 50 K in averaged images based on thermocouple measurements of the premixed laminar flame. The signal-to-noise ratio of the Stokes images were approximately 20:1 and 10:1 for the anti-Stokes images, with typical signals exceeding 25,000 and 10,000 counts, respectively. The technique is not accurate below 800 K owing to the low population density of thermally excited, indium which is probed using the Anti-Stokes beam [15]. Accordingly, temperatures reported using the NTLAF method ($\langle T \rangle$) are conditioned on $T \geq 800$ K.

Laser sheets were nominally 25 mm high, with the central 21 mm presented herein. Data were collected at the swirler exit plane and, for select cases, 15 and 25 mm above the exit plane. Averaged values for mean images, and profiles, of conditional temperature were only evaluated at locations where valid values existed in a minimum of 75 images (30% of the set). This was done to ensure convergence of the local mean values.

Planar laser-induced fluorescence of the hydroxyl radical (OH-PLIF) was imaged by exciting the A-X(1,0) $Q_1(8)$ transition at 283.636 nm. This wavelength was produced by a frequency doubled dye laser (Lambda Physik ScanMate 2) pumped by a 532 nm Nd:YAG laser (Quantel Q-smart 850) at 10 Hz. The OH-PLIF beam propagated through a series of optics forming a 1 mJ/pulse laser sheet through the imaging plane. The OH-LIF signal was

detected with an ICCD camera (Princeton PI-Max 2) through an $f_{\#}1.2$, UV transmissive lens. The signal was imaged off of a dichroic mirror with greater than 80% reflectance at wavelengths between 270 and 340 nm, which served as a broadband filter. Images of OH structures presented here are 8 mm high, filtered with a two-dimensional 5×5 median filter, corrected for ICCD dark charge, uniformity and spatially mapped to the quantified NTLAF images. The beam propagated from the right-to-left in each image, and the effects of laser absorption were measured to be negligible. No corrections were made for beam profile and no interference from Mie scattering was detected in the instantaneous measurements presented, or at 15 mm above the burner exit plane where the data were averaged. The OH-LIF signal is analysed here to qualitatively investigate the flame structure and indicate the locations of OH. These LIF signals may not be conclusively taken to represent absolute OH number density, as the LIF signal is dependent on local quenching, which is reliant on concentration of other species and hence both temperature and mixture fraction.

3. Results and Discussion

3.1. Overview of Flame Structure Features

Images of conditional temperature in swirling spray and dual-fuel flames were produced using NTLAF, performed simultaneously with OH-PLIF. Figure 1a shows a temperature typical image produced using this set-up, annotated to show critical features of the flame and the burner itself. The 'inner reaction zone' is situated above the centre of the round bluff-body. The swirling oxidant stream and the bluff-body induce a recirculation region in which the 'outer branch' of the main reaction zone is stabilised. The two

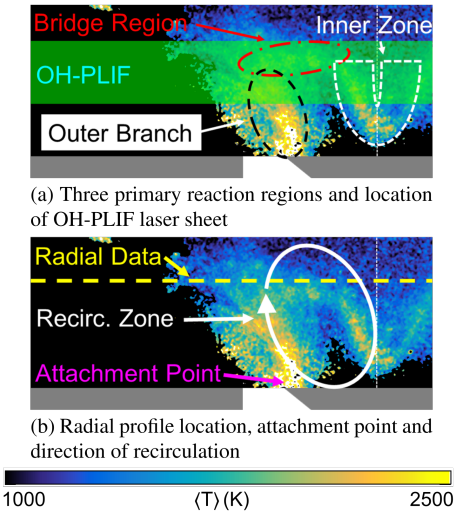

(a) Three primary reaction regions and location of OH-PLIF laser sheet

(b) Radial profile location, attachment point and direction of recirculation

Fig. 1: Annotated instantaneous image of $\langle T \rangle$ from Case S3H1 flame. The top image shows the 'inner reaction zone' (white dashed), the 'outer branch' of the reaction zone (black dashed), the 'bridge region' joining them (red dashed) as well as the OH-PLIF laser sheet (pale green). The bottom image shows the location of radial profile data (yellow dashed), 'attachment point' (indicated by magenta arrow) and the direction or induced recirculation (solid white). The grey blocks indicate the burner base, and the size of the annular swirler inlet.

reaction zones are connected by a 'bridging region'. The location of the laser sheet used for OH-PLIF is indicated in Fig. 1a, and the location of the recirculation zone and the height used to extract radial profiles are marked in Fig. 1b.

3.2. Effects of Swirling Coflow Flowrate

Radial profiles of conditional temperature and normalised OH signal for flames stabilised with cold, air-only swirling streams are presented in Fig. 2. These cases differ by the total flowrate of air only and provide complementary insight to previous studies of blow-off, and OH/CH_2O-PLIF of similar flames [6, 7]. It must be highlighted that, in all but two cases, valid conditional temperature measurements were recorded in $\geq$98% of pixels contributing

to each point in the plots for -20 < r < 3 mm. This demonstrates that observations in this range are not due intermittency effects. To visualise this, figures of the intermittency in the ensemble-averaged data for all cases are included as Supplementary Data. At the lowest flowrate (Case S1), the $\langle T \rangle$ field exhibits two peaks of similar magnitudes approximately at 8 and 17 mm from the burner centreline, representing the inner and outer reaction zones of the flame, respectively. These correspond to two peaks in the OH-LIF signal profile, located at 9 and 18 mm from the burner centreline, with a significantly higher signal from OH-LIF at the inner peak. The cold-air flowrate in this stable flame is 63% of the blow-off velocity for the n-heptane spray flame [6]. Case S4 has the highest cold air velocity, namely 88% of the blow-off velocity [6]. This case exhibits only a single peak in $\langle T \rangle$ in the outer reaction zone. The distribution of OH-LIF signal, however, displays two peaks of similar magnitudes in the two reaction zones (although these cannot be quantitatively compared to Case S1). In contrast, the Case S3 (81% of blow-off velocity [6]) demonstrates a broad, single peak in both the $\langle T \rangle$ and OH-LIF profiles. Both peak $\langle T \rangle$ and OH-LIF signal in Case S3 are located between the two peaks in Case S1 and S4. Not only is the peak value of $\langle T \rangle$ in Case S3 greater than in the other cases, it is also hotter along the burner centreline. These features suggest that Case S3 exhibits a transitional structure between the low (S1) and high (S4) flowrate cases.

Figure 3 shows false-colour images of the ensemble-averaged conditional temperature field for Cases S1, S3, and S4. All cases feature multiple reaction zones which were introduced in Fig. 1, and can be seen in instantaneous images in Fig. 4. Each case features high temperature regions above the apex

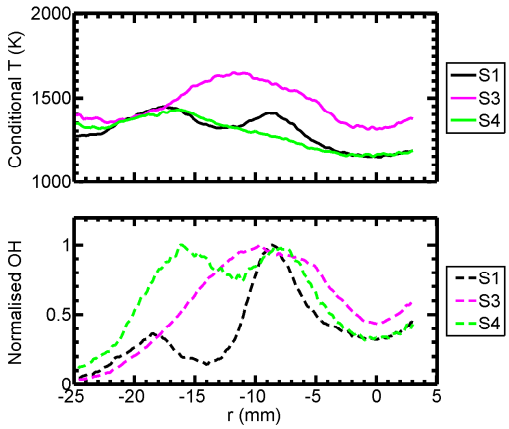

Fig. 2: Ensemble-averaged $\langle T \rangle$ profiles (solid, top) and normalised OH signal (dashed, bottom) for Cases S1, S3, and S4 taken 15 mm above the burner exit plane.

of the spray, as well as hot outer branches. The highest mean temperatures in the central reaction zone occur several millimetres above the atomiser exit plane in all cases. Interestingly, this high conditional temperature region was identified as a region of very low mean OH-LIF signal in n-heptane [6] or ethanol [2] spray flames in the same burner. The low mean OH-LIF signal in this high average-temperature region along the burner centreline indicates that the hot gases at this location are predominantly recirculating combustion products generated elsewhere in the flame, as proposed by [6]. The combination of high conditional temperature and low OH-LIF signal suggests that the reactions in the inner reaction zone are significantly diluted by hot products, under conditions which emulate exhaust gas recirculation (EGR). The narrow OH regions presented here are similar to those in previous experimental studies and large-eddy simulations (LES) using the same burner [2, 5, 6, 13, 18]. The broad regions of high temperature were also reported in previous LES studies [13, 18], although this is the first experimental evidence.

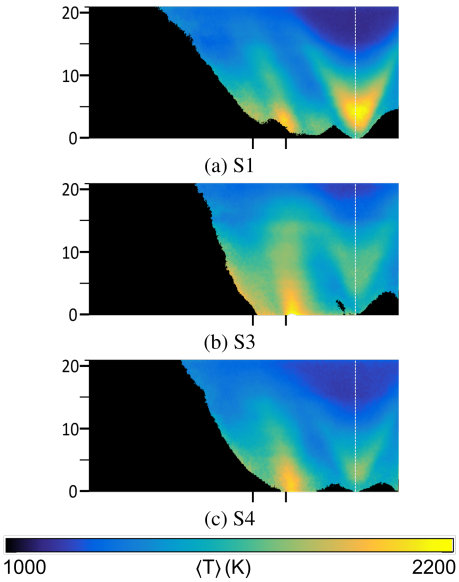

Fig. 3: False colour, ensemble-averaged $\langle T \rangle$ fields for Cases S1, S3, and S4. Burner centreline is indicated by the dashed vertical line, with exterior lines indicating the annular swirler. The left-hand edge of the images is coincident with the burner wall. Scale in millimetres. Images are 21 mm high with the base of the images at the burner base.

The highest temperatures in the outer branches occur near the outer edge of the bluff-body, which has previously been identified as the attachment point of the outer branch [2, 5, 6, 13, 18].

Comparisons of ensemble-averaged conditional temperatures show a decrease in temperature along the burner centreline with increasing cold-air flowrate (see Fig. 3). In contrast, the outer branches of the flames in Cases S3 and S4 appear more attached than in Case S1. This is due to enhanced recirculation above the bluff-body, measured previously using simultaneous laser Doppler anemometry and phase Doppler anemometry [7]. This enhanced recirculation results in a higher velocity flow from the tip of the recirculation region towards the bluff body [7], resulting in higher temperature and reduced lift-off height at the base of the outer branch. The combination of

enhanced recirculation and a larger pressure differential caused by the higher air flowrate draws fuel away from the inner reaction zone of the flames and into the recirculation region. In this recirculation region, previous LES have show that local extinction is controlled by mixing and turbulent transport rather than the scalar dissipation rate of the evaporating spray [18]. This results in lower Φ, and hence lower temperatures in the inner reaction zone. These combined effects account for the change in temperatures seen along the burner centreline and in the outer branch of the flames as the air flowrate increased.

Instantaneous images of conditional temperature in Cases S1, S3, and S4 (Fig. 4) demonstrate the same trends identified from the ensemble-averaged images in Fig. 3. Examination of instantaneous images from Case S4 reveals that the lower mean conditional temperatures, compared to Case S1, are due to intermittent lift-off of both the inner and outer reaction zones. Additionally, the higher temperature region in Case S1 causes faster evaporation of the n-heptane spray than in Cases S3 or S4, resulting in less penetration of the fuel (and less CH_2O downstream [6]) which is consistent with previously identified trends in heat-release [6].

Figure 4 shows the shift towards high peak conditional temperatures in the recirculation zone with increasing air flowrate. Noticeably, very little OH-LIF signal is evident along the burner centreline, however, local conditional temperatures exceed 1000 K in all images. The broadening of the high temperature region from Case S1 to Cases S3 and S4 is further evidence of the increase in local fuel concentration with air flowrate, and corresponds to larger OH, CH_2O, and heat-release regions identified in a previous study [6].

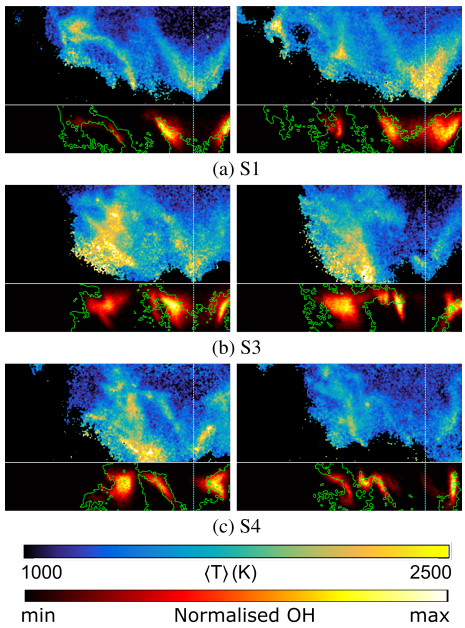

Fig. 4: Typical instantaneous $\langle T \rangle$ (21 mm tall, top) and normalised OH (8 mm tall, bottom) images from Cases S1, S3, and S4. Images extend 40 mm left of the burner centreline. Images of OH are overlaid with iso-contours of $\langle T \rangle = 1500$ K.

The comparison of these temperature images with synchronised OH-PLIF contours, shows that broad distributions of OH are centred in the high temperature regions of the inner reaction zone, but located closer to the swirling stream (to the left of the peak temperature region) in the outer branch. This suggests premixing in the inner reaction zone, whilst the outer branch behaves more like a diffusion flame. Finally, regions of hot post-combustion gases without in-plane OH structures emphasise the effects of transport in this configuration and the highly-three-dimensional nature of these flames.

3.3. Dual-Fuel Flames

Measurements of conditional temperature and OH-LIF signal in n-heptane-based dual-fuel flames complement the studies of the air-only swirling streams

[6, 7] and previous work on dual-fuel ethanol/methane flames [2]. Mean profiles are shown in Fig. 5. Profiles show data taken 15 mm above the burner base. Comparison of Case S3 and S3N1 demonstrates the effects of adding natural gas at $\Phi_{pmx} < \Phi_{LFL}$ to the swirling air stream. This results in an oxidant stream which provides an additional source of heat and precursors to the system by the addition of more fuel, but is not flammable on its own. In spite of this, the addition of NG shifts the main temperature peak towards the swirling stream and produces a smaller peak in temperature approximately 6 mm from the burner centreline. This smaller temperature peak occurs at the same location as the maximum OH-LIF signal, with a significant OH-LIF signal still present at the main temperature peak. A similar effect is seen in Case S1N1 (not shown for brevity), with a slight change in temperature accompanied by a larger normalised OH-LIF peak in the inner reaction zone of the flame. The combination of these temperature and OH-LIF signal peaks suggest multiple reaction zones (and shown later in Fig. 6), however the absolute local concentrations of OH cannot be calculated. Although consistent with previous results [2], these radial profiles alone are insufficient to understand the cause of the change in flame structure.

The addition of H_2 in Cases S3H1-S3H3 results in decrease in conditional temperature of approximately 175 K, 15 mm above the burner base (see Fig. 5). This drop in conditional temperature was not seen in Cases S1H1-S1H3 (not shown for brevity). The magnitude of this decrease in temperature does not change with the addition of further H_2 beyond that of Case S3H1, however, increasing Φ_{pmx} shifts the peak temperature away from the centreline, with a second distinct temperature peak evident in Case S3H3

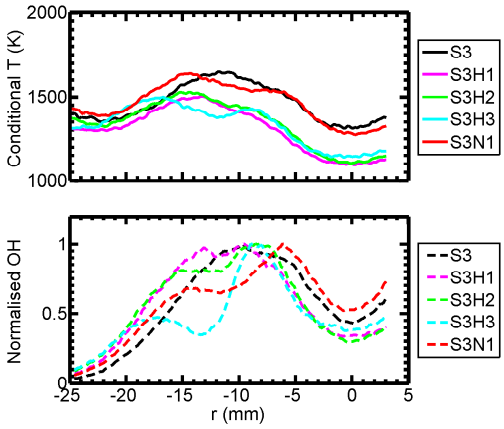

Fig. 5: Ensemble-averaged $\langle T \rangle$ profiles (solid, top) and normalised OH signal (dashed, bottom) for the dual-fuel cases taken 15 mm above the burner base for S3-based cases.

($\Phi_{pmx} > \Phi_{LFL}$). Similar to the addition of NG to the swirling coflow stream, the addition of H_2 results in shifting the OH-LIF peak towards the centreline, with a second OH-LIF peak forming in the outer branch of Case S3H3. In contrast to Case S3N1, the coflowing stream in Case S3H3 is flammable and may sustain combustion, creating a hot, swirling coflow with H_2O.

Figure 6a shows the mean conditional temperature field of Case S3N1, which may be compared with the cold air Case S3 (previously shown in Fig. 3b). The shift in peak conditional temperature with the addition of NG at $\Phi_{pmx} = 0.18 < \Phi_{LFL}$ (see Fig. 5) is evident by comparing the images in the two figures, with the peak temperature shifting from the central, inner reaction zone in Case S3 to the attachment point in the outer branch. This addition of NG does not reduce the size of the high temperature region in the inner zone.

The peak temperatures in Cases S3N1, S3H1, and S3H2 (the final case omitted for brevity) occur in the outer branches, despite $\Phi_{pmx} < \Phi_{LFL}$ in all

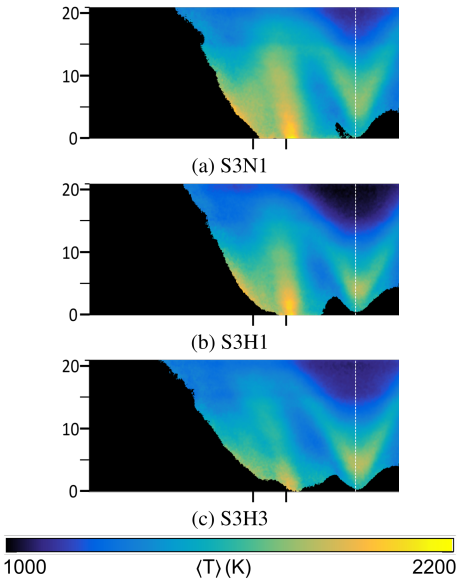

Fig. 6: False colour, ensemble-averaged $\langle T \rangle$ fields for Cases S3N1, S3H1, and S3H3. Burner centreline is indicated by the dashed vertical line, with short lines indicating the annular swirler. Burner inner walls are at the left-hand edge of the images. Scale in millimetres. Images are 21 mm high with the base of the images at the burner base.

three cases (see Fig. 6). This indicates that combustion in the outer branch is fuelled by a mixture of NG or H_2, and vaporised n-heptane. This vaporised n-heptane is transported to the outer branch through the positive mean radial velocity in the lower part of the recirculation zone, and by turbulent transport. Furthermore, the addition of H_2 reduces the size of the highest temperature region in the inner reaction zone, for both $\Phi_{pmx} < \Phi_{LFL}$ and $\Phi_{pmx} > \Phi_{LFL}$, which is not seen in Case S3N1. The outer reaction branches of Cases S3N1, S3H1, and S3H2 include large regions of high $\langle T \rangle$. These regions are cooler in Case S3H3, with higher temperatures in the inner reaction zone compared to the other cases. Furthermore, the flame in Case S3H3 spreads faster than the other cases, consistent with Fig. 5.

Instantaneous images of conditional temperature from Cases S3N1, S3H1,

and S3H3 are shown in Fig. 7. These may be compared to the images of Case S3 in Fig. 4b. Images of Case S3N1 in Fig. 7a demonstrate that the high temperature region of the flame near the spray cone has a similar shape to that identified in Case S3, with an increase in temperature due to the additional fuel. Similarly, high temperature regions in the outer branch of Case S3N1 have a similar appearance to those in Case S3, as suggested from Fig. 5. These comparisons are similar to those which may be drawn from images of Case S3H1. In contrast to these effects, typical images of $\langle T \rangle$ in Case S3H3 in Fig. 7c show the hotter flame near the apex of the spray, in comparison to the outer branch of the flame. This shift occurs with an increased prevalence of lift-off and intermittent branches of hot gas extending to the far side of the swirling stream, albeit without indications of in-plane OH structures. This intermittency explains the cooler mean conditional temperatures in Fig. 6. These trends are phenomenologically similar to that of OH-LIF field with the addition of gaseous CH_4 to ethanol spray flames in the same configuration [2], as well as LES which showed that local extinction is more prevalent in the outer branches [18].

Analyses of Figs. 5-7 demonstrate, and quantify, the effects of heat-releasing, swirling coflow streams on n-heptane spray flames. These show that the regions of highest temperature shift from above the spray apex to the outer branch of the flame ($\Phi_{pmx} < \Phi_{LFL}$), and back again $\Phi_{pmx} > \Phi_{LFL}$, with increasing Φ_{pmx}. The addition of H_2 results in a smaller flame above the spray apex which is significantly cooler above the inner reaction zone. These trends are qualitatively similar to the changes due to CH_4 addition [2].

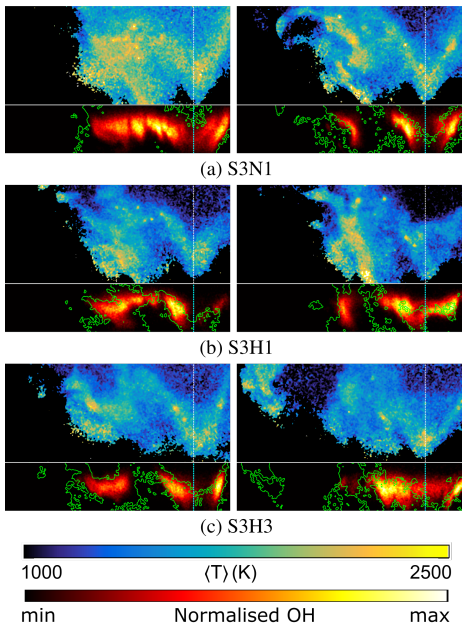

Fig. 7: Typical instantaneous $\langle T \rangle$ (21 mm tall, top) and normalised OH (8 mm tall, bottom) images from Cases S3N1, S3H1 and S3H3. Images extend 40 mm left of the burner centreline. Images of OH are overlaid with iso-contours of $\langle T \rangle = 1500$ K.

4. Conclusions

Conditional temperatures have been measured in swirling, n-heptane spray flames using non-linear excitation regime two-line atomic fluorescence (NTLAF) of indium. Conditional temperature measurements quantify the effects of increasing the flowrate of a cold, swirling air stream and the effects of fuel addition into the swirling stream. Increasing the cold, swirling flowrate towards blow-off results in stronger recirculation, in accordance with previous velocity measurements [7], drawing fuel away from the inner reaction zone and towards the outer branch of the flame. This results in a cooler inner reaction zone and increased temperatures at the bluff body, consistent with previous observations of broadening heat-release regions [6]. The addition of

gaseous fuels to the swirling stream adds heat to the system, however, the addition of H_2 results in a smaller high temperature region above the spray apex and cooler temperatures 15 mm above the burner base. The high temperature region above the spray apex is largely unaffected by the addition of NG. Increasing Φ_{pmx} towards Φ_{LFL} shifts the high temperature region of the flame near the burner base towards the outer flame branch. Exceeding Φ_{LFL}, however, produces an additional temperature peak corresponding to a premixed flame and the region of highest conditional temperature returns to the burner centreline above the spray apex, but increases the propensity for lift-off. The data collected in this study also provide a series of challenging test-cases for the validation of numerical models for liquid fuel combustion.

Acknowledgements

The authors thank Mr Amir Rowhani and Dr Alfonso Chinnici for their assistance during experimental data collection. The authors acknowledge support from The University of Adelaide and the University of Cambridge. M.J.E., P.R.M. and B.B.D. acknowledge financial support from the Australian Research Council (ARC) Discovery (DP and DECRA) grant scheme, and the United States Asian Office for Aerospace Research and Development (AOARD). J.A.M.S. acknowledges a start-up grant from the Department of Engineering, University of Cambridge.

References

[1] A. R. Masri, Combust. Sci. Technol. 188 (2016) 1619–1639.

[2] J. Sidey, E. Mastorakos, Proc. Combust. Inst. 36 (2017) 1721–1727.

[3] H. Correia Rodrigues, M. J. Tummers, E. H. van Veen, D. J. Roekaerts, Combust. Flame 162 (2015) 759–773.

[4] L. Ma, D. Roekaerts, Proc. Combust. Inst. 36 (2016) 2603–2613.

[5] D. E. Cavaliere, J. Kariuki, E. Mastorakos, Flow, Turbul. Combust. 91 (2013) 347–372.

[6] R. Yuan, J. Kariuki, A. Dowlut, R. Balachandran, E. Mastorakos, Proc. Combust. Inst. 35 (2015) 1649–1656.

[7] R. Yuan, Measurements in Swirl-stabilised Spray Flames at Blow-off, Ph.D. thesis, University of Cambridge, 2015.

[8] G. K. Lilik, H. Zhang, J. M. Herreros, D. C. Haworth, A. L. Boehman, Int. J. Hydrogen Energ. 35 (2010) 4382–4398.

[9] A. J. Nord, J. T. Hwang, W. F. Northrop, J. Energy Resour. Technol. 139 (2017). Paper 022204.

[10] M. R. Bothien, D. A. Pennell, M. Zajadatz, K. Döbbeling, in: ASME Turbo Expo 2013: Turbine Technical Conference and Exposition. Paper GT2013-95693.

[11] S. B. Pope, Proc. Combust. Inst. 34 (2013) 1–31.

[12] B. F. Magnussen, in: ECCOMAS thematic conference on computational combustion, Lisbon, Portugal. June 21–24, 2005.

[13] A. Tyliszczak, D. E. Cavaliere, E. Mastorakos, Flow, Turbul. Combust. 92 (2014) 237–267.

[14] H. Le, Y. Liu, M. S. Mannan, Ind. Eng. Chem. Res. 52 (2013) 1372–1378.

[15] P. R. Medwell, Q. N. Chan, P. A. M. Kalt, Z. T. Alwahabi, B. B. Dally, G. J. Nathan, Appl. Spectrosc. 64 (2010) 173–176.

[16] Q. N. Chan, P. R. Medwell, B. B. Dally, Z. T. Alwahabi, G. J. Nathan, Appl. Spectrosc. 66 (2012) 803–809.

[17] D. Gu, Z. Sun, G. J. Nathan, P. R. Medwell, Z. T. Alwahabi, B. B. Dally, Combust. Flame 167 (2016) 481 – 493.

[18] A. Giusti, E. Mastorakos, Proc. Combust. Inst. 36 (2017) 2625–2632.

List of Figures